AIMS Materials Science, 7(2): 144–156.
DOI: 10.3934/matersci.2020.2.144
Received: 29 January 2020
Accepted: 31 March 2020
Published: 07 April 2020

http://www.aimspress.com/journal/Materials

Research article

Hydrogen generation performance of Al–20at%Ca alloy synthesized by mechanical alloying

A. G. Hernández-Torres[1], J.L. López-Miranda[2], I. Santos-Ramos[3] and G. Rosas[3,*]

[1] Facultad de Química, UNAM circuito exterior, Ciudad Universitaria, 04510, México, D.F.
[2] Centro de Física Aplicada y Tecnología Avanzada, UNAM, Boulevar Juriquilla 3001, Santiago de Querétaro, QRO,76230, México
[3] Instituto de Investigaciones en Metalurgia y Materiales, UMSNH, edificio U, ciudad universitaria, C.P. 58060, Morelia, Michoacán, México

* **Correspondence:** Email: grtrejo@yahoo07.com.mx, grtrejo@umich.mx.

Abstract: In this study, the Al–20at%Ca alloy was synthesized by mechanical alloy from the elemental powder mixture. Subsequently, the alloy particles were reacted at room temperature to determine the amount of hydrogen released. For these purposes, the powders reacted with different types of water, such as distilled water, tap water, and seawater, and also in the presence of NaCl and CaO additives. Both milled samples and reaction powders were analyzed by X-ray diffraction (XRD), scanning electron microscopy (SEM), transmission electron microscopy (TEM), FT-IR, and Raman spectroscopy (RS). The XRD patterns of the powders prepared show a nanocrystalline alloy consisting of a solid-cubic solution of Al and the tetragonal intermetallic phase $CaAl_4$. Studies of XRD and SEM, as well as direct measurements of H_2, indicated that the best results of H_2 generation were obtained when the alloy reacts with distilled water. Both NaCl and CaO additives improve hydrogen generation, reaching 100% efficiency in distilled water and seawater, and without induction time. Samples with a combination of NaCl and distilled water showed the best reaction times to generate the entire theoretical amount of hydrogen. The XRD and DSC–TGA standards also confirmed the presence of bayerite $Al(OH)_3$ as a secondary reaction product.

Keywords: hydrogen generation; intermetallic; nanostructured materials; mechanical alloying; microstructure; X-ray diffraction; scanning electron microscopy

1. Introduction

Hydrogen element is an essential fuel for potential use in clean and emission-free transport applications [1,2]. One of the main challenges of hydrogen technologies is its storage capacity [3–5]. However, an alternative to hydrogen storage is the in-situ H_2 generation and feeding on-demand in a hydrogen fuel cell. In this context, aluminum and its alloys have been extensively investigated as useful materials for its reaction with water to release hydrogen [6–8]. Elemental aluminum has difficulty reacting at room temperature with water due to the formation of a passive layer of aluminum oxide [9]. Therefore, to improve the efficiency of the hydrogen reaction, catalytic substances are required that influence the reaction rate by the passive layer elimination. In this sense, several additives such as NaOH [10], KOH [11], NaCl [12], among others [13–14], have been successfully tested. Recently the aluminum has been combining with carbon [12,15] and oxides [16].

Another way to improve the Al reaction with water has been its alloy with Ga and adding several low-melting-point elements such as In, Sn, Zn, and Bi obtaining excellent reaction efficiencies [17]. Also, elements such as Mg, Fe, Co, Ni, have been explored [18–21]. These alloys have carried out by the continuous casting method. However, some elements increase the production cost of the material.

Moreover, in some investigations for the reaction to occur, the temperature must rise [18,22]. Other evaluated production methods include biological and electrochemical processes [23]. However, the biological processes have relatively low efficiency, and the electrochemical methods have a high production cost [24,25].

Alloy and mechanical activation of Al with various elements have also been a successful alternative [26–28]. Mechanical milling is a simple and relatively low-cost method that produces nanocrystalline powder alloys [29]. During the ball milling process, a large number of crystalline defects such as vacancies and dislocations are generated that accumulate a large amount of energy and increase internal stresses in the material. Nanocrystals in the material increase the grain surface area, thus raising the area available for the reaction, that, in addition to the accumulated energy, are structural characteristics that favor the diffusion and reactivity of the chemical species. The effect of increasing surface area on Al's reaction with water was reported in the past. For example, nanoaluminum particles reacted completely to produce bayerite at low temperatures, while microparticles did not [30]. In all cases, the reaction for the hydrogen generation is carried out in three steps: induction time, rapid generation, and passivation. The induction time is the period in which the reaction begins, from the moment the reagents come into contact until the first hydrogen bubble appears [21]. An objective of the new technologies for hydrogen generation is to find the right conditions (maybe room temperature) and appropriated materials so that the induction time was zero or almost zero.

On the other hand, Al-based intermetallic compounds are of our interest because of the hydrogen environmental fracture that affects them [31]. In this process, the Al of the intermetallic compound reacts spontaneously with the water vapor in the air, causing to release of hydrogen. Then, hydrogen releasing causes cleavage fracture of the material increases the surface area, improving the conditions for the reaction of the intermetallic compound with water. Thus, Al-based intermetallic compounds must be explored for these purposes. Thus, in this study, we present the results obtained

from the reaction of the Al-based alloy (Al–20at%Ca) with different types of water and in the presence of NaCl and CaO additives. The alloy mixture was obtained by high-energy ball milling in a two-phase region consisting of a solid solution of aluminum, Al[Ca], and the intermetallic phase $CaAl_4$, according to the equilibrium phase diagram.

2. Materials and methods

2.1. Materials

In the present work: Al powder (99.5% purity), Ca powder (99.5% purity), NaCl (99.0% purity), and CaO (96% purity) supplied from Alpha Aesar are used as starting materials.

2.2. Alloy preparation

A binary alloy with a nominal composition of Al–20at%Ca was prepared by high-energy ball milling starting from elemental powders. In a container of hardened steel were loaded 3 g of elemental powders and two hardened stainless-steel balls (8.4 g) to give a ball-to-powder mass ratio of 2:8. To form a nanocrystalline alloy, Al and Ca powders were subject to high-energy ball milling in a SPEX 8000 M mill/mixer for 3, 6, and 9 h. During operation, an Ar atmosphere was used to avoid the oxidation of the powders. Then, the alloy particles were exposed to their reaction with different types of water: distilled water, tap water, and seawater. CaO and NaCl additives (10 wt%) were used to improve the response of the synthesized powders with different types of water. A ball-milling process was conducted for 30 min to homogenize the as-synthesized alloy with the additives.

2.3. Hydrogen generation properties measurements

During the reaction of the powders and water, the amount of hydrogen released was measured by the method described previously in [21] with minor modifications. Al–20at%Ca alloy particles reacted with different types of water (tap water, natural seawater, or distilled water) inside a 100 ml Kitasato flask. The hydrogen produced by this reaction was taken to a 250 mL distillation flask, inverted and filled with water. This container also served as a water trap for temperature rise during the reaction. The last paragraph constituted the experimental modification with respect to [21]. Water evacuated by hydrogen bubbles in the distillation flask was captured in a 250 mL burette. In each experimental sample, the mass of the Al element contained in the alloy was equivalent to producing 250 mL of H_2 under standard conditions (298 K and 1 atm) with excess water. The formation of the first bubble inside the distillation flask indicates the initial time for H_2 generation. At the end of each experiment, the volume change of the inverted burette was measured to determine the amount of hydrogen released. In addition, the induction time, generation time and total amount of hydrogen released were recorded.

2.4. Microstructural characterization

In addition to direct measurements of H_2 release, evidence of the reaction between Al and water can be observed through morphological and chemical changes in the powders after the reaction. Microstructural characterization of particles with and without additives was performed by X-ray diffraction (XRD, Siemens D5000 X-ray diffractometer) and scanning electron microscopy (SEM, JEOL JSM 2400). In addition, energy dispersive spectroscopy (EDS) analysis was performed on all milled samples to determine their chemical composition. Differential scanning calorimetry analysis (DSC) and thermogravimetric analysis (TGA) was performed using a TA Instruments SDT Q600.

3. Results and discussion

Figure 1a displays the XRD pattern of the un-milled sample, which contains only the typical diffraction peaks of the Al and Ca. Figure 1b,c shows the XRD patterns of as-milled (Al, Ca) powders after 6 h, and 9 h, respectively. These powders were used in this work for hydrogen generation. The diffraction peaks identified in both XRD patterns confirmed the formation of both Al[Ca] cubic solid solution and the $CaAl_4$ tetragonal intermetallic phase after 6 h of mechanical milling. The observed phases in the XRD patterns are in good agreement with the Al–Ca phase diagram for the nominal alloy composition used in this work. The crystal size calculated using the Debye–Sherrer equation from the Al (111) crystallographic plane (FWHM) was 17 nm, which confirms the formation of a nanocrystalline alloy [32,33]. According to the Miedema model, the enthalpy of formation for the Al–20at%Ca is negative (−8.65 kJ/mol), which indicates that a mechanical alloy process can form the $CaAl_4$ phase. A negative enthalpy of formation induces a significant driving force and nucleation due to the relatively simple crystalline structure. The dissolution of Ca in Al is due to crystalline defects induced by milling. All these defects provide the highest percentage of solubility of the solute element in the structure of Al. These defects may include vacancies, dislocations, and grain boundaries, which also participate in the activation of the powders for their reaction with water. On the other hand, ball milling of the additives with the alloyed powders intends to induce a higher number of active sites for their reaction with water.

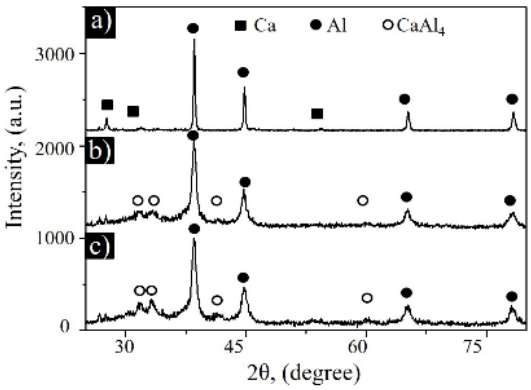

Figure 1. (a) XRD pattern of the un-milled sample with diffraction peaks of the starting powders (Al, Ca). XRD patterns of as-milled powders after (b) 6 h and, (c) 9 h.

Figure 2a shows an SEM micrograph illustrating the morphological characteristics of the powders milled for 6 h. The sample exhibits a relatively narrow particle size distribution. The agglomerates observed were formed as a result of these steps: plastic deformation, welding, and fracture that repeatedly occurred in the particles during the ball-milling process. Figure 2b shows the EDS chemical analysis of the sample, indicating the presence of signals of Al, Ca and small amounts of O. The O presences is attributed to the slight oxidation on the particle surface of both metals being approximately 0.5 wt% [34].

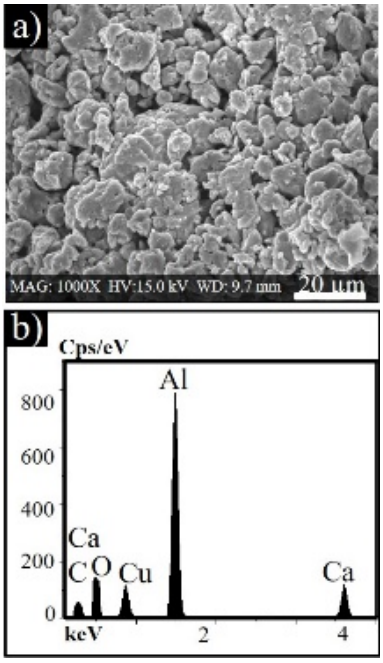

Figure 2. (a) SEM micrograph of the powders after 6 h high-energy ball milling, (b) EDS analysis of the same particles showing the chemical composition.

Figure 3 shows the curves of hydrogen generation of the Al–20at%Ca powder as a function of processing time in the different water types. From the graph, we can notice that the use of distilled water indicates the best results for hydrogen generation, followed by the use of tap water and seawater. Similar results were obtained by Wang et al. [35], getting better results in distilled water in comparison with deionized water and tap water. On the contrary, Gai et al. [36] find that the Al reaction with tap water and deionized water is faster than distilled water and seawater. Mag et al. [37] obtained 10% more hydrogen production with seawater, compared with deionized water attribute to the enriched chlorine ions, which accelerate the dissolution reaction of the passivation layer on the Al surface. However, in general, the results of hydrogen generation after the reaction of Al with only different types of water are low; that is why over the years, several additives have used for the reaction activation. In addition, the physicochemical properties of seawater are different from the tap or distilled water. Properties such as density, viscosity, and bacterial content, can make the chemistry of seawater complex, so its reaction to generate hydrogen is also.

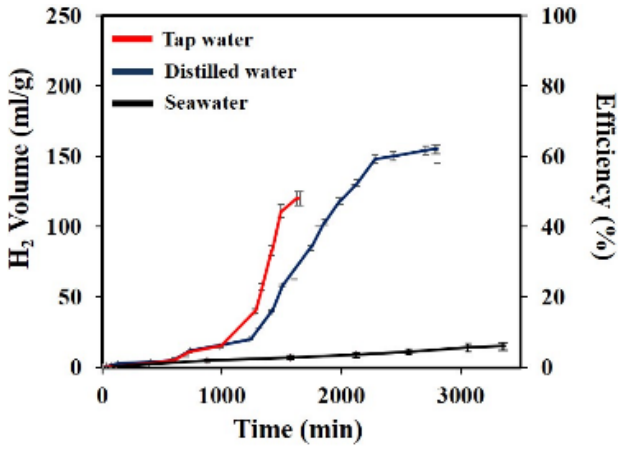

Figure 3. Hydrogen generation of as-milled powders after its reaction under different water types.

XRD analyses were carried out to know the by-products derived from the hydrogen generation reaction between the milled powders and the different types of water. Figure 4 shows the X-ray diffraction patterns to confirm the existence of reaction products as a result of the generation of hydrogen with the use of the intermetallic phase as an internal additive and different types of water.

Figure 4a shows the X-ray diffraction pattern of the powders after their reaction with distilled water. The analysis of this pattern shows the absence of the $CaAl_4$ intermetallic phase. These findings reveal that the intermetallic phase reacts entirely with water. Therefore, the intermetallic compound decomposes, functioning as an additive in the material. As mentioned earlier, intermetallic materials react spontaneously with water vapor in the air to produce ambient hydrogen [38]. As appreciated, there are small amounts of the starting phase Al[Ca] in the XRD pattern indicating partial reaction with distilled water to produce hydrogen. These results are in good agreement with the results of direct H_2 generation measurements. Additionally, diffraction peaks of the compounds derived from the reaction such as aluminum hydroxide ($Al(OH)_3$) with the monoclinic phase and also cubic calcium carbonate ($CaCO_3$) were identified. $Al(OH)_3$ compound (bayerite) appears according to the chemical Eq 1 [39].

$$2Al + 6H_2O = 2Al(OH)_3 + 3H_2 \quad (1)$$

where, either Al of the solid solution Al[Ca] or from the intermetallic compound $CaAl_4$ react with distilled water releasing hydrogen to form bayerite compound. On the other hand, the observed $CaCO_3$ is due to CaO reaction with CO_2 environmental, according to the chemical Eq 2 [40,41].

$$CaO + CO_2 = CaCO_3 \quad (2)$$

Figure 4b shows the XRD pattern of the reacted particles in contact with tap water. The diffraction peaks of the same compounds observed in the as-milled alloy (Al[Ca] cubic and $CaAl_4$) were identified. The presence of the starting phases indicates a reduced efficiency of reaction with tap water, which agrees well with the results of the direct measurements of H_2. These results could be due to the presence of several ions dissociated in tap water. This outcome leads to a lower number of hydroxyl ions and neutral values of pH and affects their reaction with the alloy mixture [20].

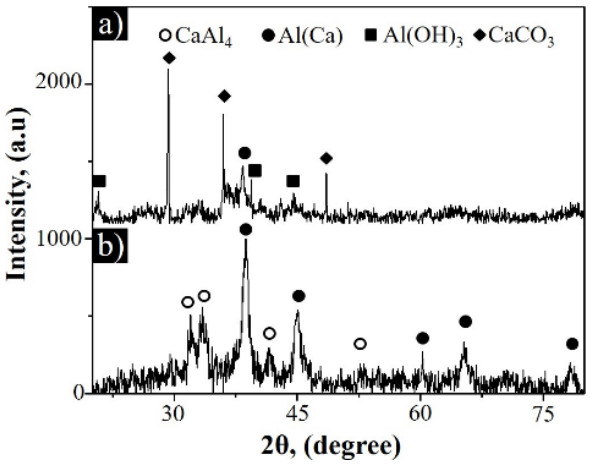

Figure 4. XRD patterns of the reactant particles in contact with (a) distilled water and, (b) tap water.

Figure 5 shows the graph of the amount of hydrogen released in the Al–20at%Ca alloy reacting with distilled water and seawater using NaCl and CaO, respectively. It is observed from the curve that the total theoretical yield of hydrogen according to the mass used in these experiments (250 mL) was achieved with the NaCl additive and by using distilled water. Furthermore, the induction time was 0 s, and a higher rate of reaction was obtained in the comparison to the use of seawater + CaO mixture. These findings are comparable to those achieved by using extreme experimental conditions, such as the use of toxic substances as NaOH, KOH or temperature [10–11,18,42].

The sodium chloride salt is highly soluble in water and activates the corrosion of aluminum by promoting the mobility of ions and the transfer of electrical charges [42]. Seawater itself contains NaCl. However, it has been reported that the corrosion process improves when NaCl is milled with the powders before the reaction occurs, leading to a small particle size distribution. Also, when NaCl has increased, the response of the particles to the reaction with water increases [43].

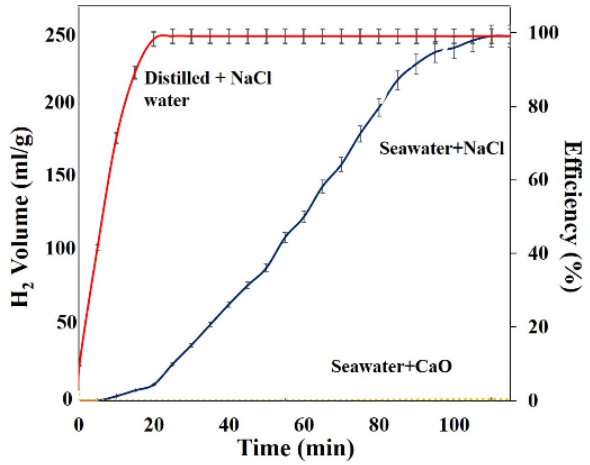

Figure 5. Graph showing the amount of hydrogen released from the Al–20at%Ca alloy reacting with distilled water and seawater with the use of NaCl and CaO additives.

Figures 6 show the XRD patterns of the reaction powders in contact with seawater or distilled water and with the addition of NaCl, respectively. In both XRD patterns, some evidence of the starting materials (i.e., Al[Ca] and $CaAl_4$) was not displayed. These results indicate their complete reaction with water to produce H_2. From the patterns, the presence of the monoclinic phase $Al(OH)_3$ was also determined, which means that the starting materials react to produce hydrogen with water according to the chemical Eq 1. Moreover, XRD peaks of the NaCl and $CaCO_3$ compounds were also identified. NaCl appears when the sample is dried for its structural characterization. The milled powders are activated for the hydrogen generation reaction due to the crystal size reduction and the increment in internal stresses. Thus, the presence of NaCl additions is useful for obtaining better H_2 generation in the Al–20at%Ca alloy. The hydrogen generation resulting from seawater is a surprising result. It should be considered that in seawater, there is a slight reduction of the OH and H ions, which are occupied by the solvation of metallic salts dissolved in the seawater (3.5 g/L) as compared to the distilled water. In addition, seawater has a higher density, viscosity, and contains organic matter compared to distilled water. These differences in the physicochemical properties of water may also be responsible for the delayed rate of hydrogen generation in seawater. The last can be seen as if there was more water available in distilled water than in the seawater for the reaction with the powders and H_2 generation. On the other hand, the amounts of ions dissolved in the seawater could be acting as agents of charge mobility that, in some way, aids in the process chemistry of hydrogen generation. Obviously, from the commercial point of view, the best result obtained in this work was those achieved with seawater and NaCl additive.

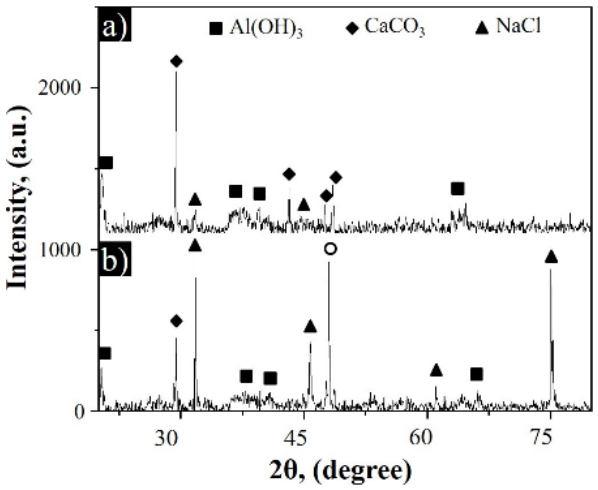

Figure 6. XRD patterns of the Al–20at%Ca reaction powders with the addition of NaCl in contact with (a) seawater and, (b) distilled water.

Figures 7a,b show the SEM powders morphology and their corresponding EDS analysis spectra after their reaction with distilled water and seawater and in the presence of NaCl, respectively. As can be seen from micrographs, the agglomerates show signs of reaction on their surface, for example, roughness, in addition to a smaller particle size in comparison with the starting material (Figure 2).

EDS chemical analysis performed on the samples in the case of deionized water (Figure 7c) shows only the alloy elements (i.e., Al and Ca) with the presence of high oxygen counts attribute to the reaction by-products ($Al(OH)_3$). EDS spectrum of the sample reacted with seawater (Figure 7d), shows elements from the seawater ions (S, Cl, Na, and Mg) and the alloy (Al and Ca). Furthermore, there are also high oxygen counts that can be related to the formation of the $Al(OH)_3$ compound. The presence of the $Al(OH)_3$ compound is directly related to H_2 generation, as previously determined by the XRD patterns.

In the past, reports that the intermetallic materials react spontaneously with water to release hydrogen [21]. The hydrogen generated reduces cohesive forces in the solid to provoke cleavage fracture [31]. In this way, the reduction in particle sizes due to the hydrogen fracturing exposes a new surface area to the reaction with water, improving hydrogen generation. That is, the same intermetallic material is acting as an additive within the material.

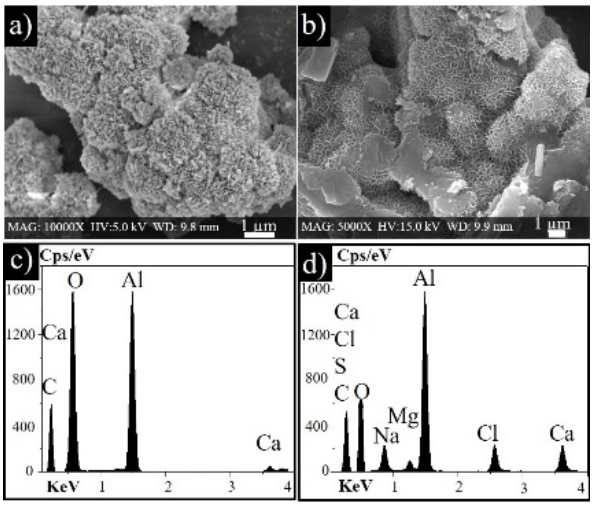

Figure 7. SEM micrographs of the Al–20at%Ca reaction powders with the addition of NaCl in contact with (a) distilled water and (b) seawater, (c) and (d) their corresponding EDS analysis.

DSC and TGA experiments obtained after the reaction of the powder with distilled water and seawater and in the presence of NaCl, respectively, are shown in Figures 8a,b. As observed in both curves, an endothermic peak situated around 294 ºC corresponding to the dehydration of bayerite appear [44] according to the Eq 3. The integrated area of the peak is more prominent in the sample with distilled water than in the seawater that is in good agreement with the results of the direct measurement of H_2.

$$2Al(OH)_3 = Al_2O_3 + 3H_2O \quad (3)$$

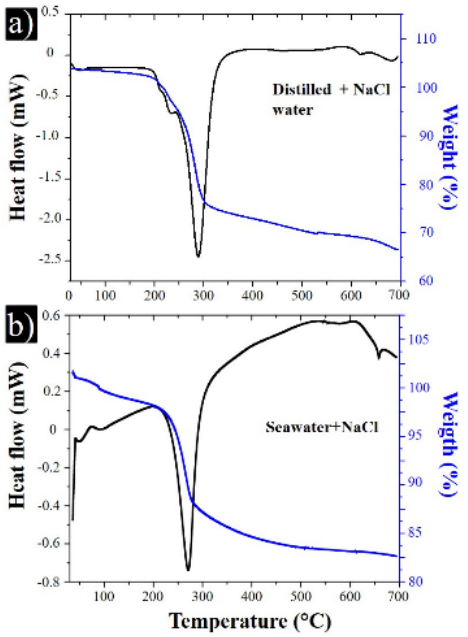

Figure 8. DSC–TGA analysis of the powders after reacting using NaCl and different types of water (a) distilled water, and (b) seawater.

Figure 9 shows the micro-Raman spectra for the resulting sample obtained from the reaction of Al–Ca with distilled water using the additive NaCl. The spectrum indicates the presence of bayerite phase, $Al(OH)_3$, and $CaCO_3$. The presence of $Al(OH)_3$ in the Raman spectra appears as a solid byproduct during the powder's alloy reaction with water.

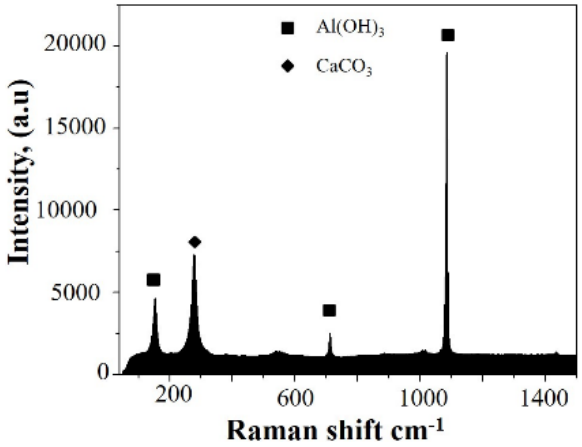

Figure 9. Raman spectrum of the reacting particles with distilled water using NaCl as additive.

4. Conclusions

In summary, in this investigation, the Al–20at%Ca alloy prepared by high-energy ball milling was evaluated as hydrogen generation material. XRD and SEM studies, as well as direct

measurements of H_2, indicate that the use of distilled water was better than seawater and tap water. NaCl additions to the intermetallic character alloy improve hydrogen generation in distilled water, reaching 100% efficiency and registering zero induction time. The hydrogen generation from the alloy was not as flattering in samples with the use of seawater and NaCl additive. X-ray diffraction shows that the $Al(OH)_3$ compound was the main byproduct of aluminum corrosion.

Acknowledgements

The authors want to thank for financial support from Consejo Nacional de Ciencia y Tecnología (CONACYT, México). In special for the Doctoral project to A.G. Hernandez-Torres (CVU 335904) is gratefully acknowledged.

Conflict of interests

All authors declare no conflicts of interest in this paper.

References

1. Chi J, Yu H (2018) Water electrolysis based on renewable energy for hydrogen production. *Chinese J Catal* 39: 390–394.
2. Boran A, Erkan S, Eroglu I (2018) Hydrogen generation from solid state NaBH4 by using FeCl3 catalyst for portable proton exchange membrane fuel cell applications. *Int J Hydrogen Energ* 44: 18915–18926.
3. Zhang F, Zhao P, Niu M, et al. (2016) The survey of key technologies in hydrogen energy storage. *Int J Hydrogen Energ* 41: 14535–14552.
4. Ancona MA, Antonioni G, Branchini L, et al. (2016) Renewable energy storage system based on a power-to-gas conversion process. *Energ Procedia* 101: 854–861.
5. Kotowicz J, Bartela Ł, Węcel D, et al. (2017) Hydrogen generator characteristics for storage of renewably-generated energy. *Energy* 118: 156–171.
6. Czech E, Troczynski T (2010) Hydrogen generation through massive corrosion of deformed aluminum in water. International journal of hydrogen energy. *Int J Hydrogen Energ* 35: 1029–1037.
7. Soler L, Macanás J, Muñoz M, et al. (2007) Synergistic hydrogen generation from aluminum, aluminum alloys and sodium borohydride in aqueous solutions. *Int J Hydrogen Energ* 32: 4702–4710.
8. Mahmoodi K, Alinejad B (2010) Enhancement of hydrogen generation rate in reaction of aluminum with water. *Int J Hydrogen Energ* 35: 5227–5232.
9. Flores-Chan JE, Bedolla-Jacuinde A, Patiño-Carachure C, et al. (2018) Corrosion study of Al–Fe (20 wt-%) alloy in artificial sea water with NaOH additions. *Can Metall Quart* 57: 201–209.
10. Hurtubise DW, Klosterman DA, Morgan AB (2018) Development and demonstration of a deployable apparatus for generating hydrogen from the hydrolysis of aluminum via sodium hydroxide. *Int J Hydrogen Energ* 43: 6777–6788.

11. Porciúncula CB, Marcilio NR, Tessaro IC, et al. (2012) Production of hydrogen in the reaction between aluminum and water in the presence of NaOH and KOH. *Braz J Chem Eng* 29: 337–348.
12. Al Bacha S, Zakhour M, Nakhl M, et al. (2020) Effect of ball milling in presence of additives (Graphite, $AlCl_3$, $MgCl_2$ and NaCl) on the hydrolysis performances of $Mg_{17}Al_{12}$. *Int J Hydrogen Energ* 45: 6102–6109.
13. Razavi-Tousi SS, Szpunar JA (2016) Effect of addition of water-soluble salts on the hydrogen generation of aluminum in reaction with hot water. *J Alloy Compd* 679: 364–374.
14. Li F, Zhu B, Sun Y, et al. (2017) Hydrogen generation by means of the combustion of aluminum powder/sodium borohydride in steam. *Int J Hydrogen Energ* 42: 3804–3812.
15. Xiao F, Yang R, Gao W, et al. (2020) Effect of carbon materials and bismuth particle size on hydrogen generation using aluminum-based composites. *J Alloy Compd* 817: 152800.
16. Guan X, Zhou Z, Luo P, et al. (2019) Hydrogen generation from the reaction of Al-based composites activated by low-melting-point metals/oxides/salts with water. *Energy* 188: 116107.
17. Qiao D, Lu Y, Tang Z, et al. (2019) The superior hydrogen-generation performance of multi-component Al alloys by the hydrolysis reaction. *Int J Hydrogen Energ* 44: 3527–3537.
18. Yang B, Zhu J, Jiang T, et al. (2017) Effect of heat treatment on AlMgGaInSn alloy for hydrogen generation through hydrolysis reaction. *Int J Hydrogen Energ* 42: 24393–24403.
19. Du BD, He TT, Liu GL, et al. (2018) Al-water reactivity of AlMgGaInSn alloys used for hydraulic fracturing tools. *Int J Hydrogen Energ* 43: 7201–7215.
20. Liang J, Gao LJ, Miao NN, et al. (2016) Hydrogen generation by reaction of Al–M (M = Fe, Co, Ni) with water. *Energy* 113: 282–287.
21. López-Miranda JL, Rosas G (2016) Hydrogen generation by aluminum hydrolysis using the Fe2Al5 intermetallic compound. *Int J Hydrogen Energ* 41: 4054–4059.
22. Brisse A, Schefold J, Zahid M (2008) High temperature water electrolysis in solid oxide cells. *Int J Hydrogen Energ* 33: 5375–5382.
23. Ilyukhina AV, Kravchenko OV, Bulychev BM (2017) Studies on microstructure of activated aluminum and its hydrogen generation properties in aluminum/water reaction. *J Alloy Compd* 690: 321–329.
24. Acar C, Dincer I (2019) Review and evaluation of hydrogen production options for better environment. *J Clean Prod* 218: 835–849.
25. Ho CY, Huang CH (2016) Enhancement of hydrogen generation using waste aluminum cans hydrolysis in low alkaline de-ionized water. *Int J Hydrogen Energ* 41: 3741–3747.
26. Du Preez, SP, Bessarabov DG (2018) Hydrogen generation by the hydrolysis of mechanochemically activated aluminum-tin-indium composites in pure water. *Int J Hydrogen Energ* 43: 21398–21413.
27. Du Preez SP, Bessarabov DG. (2019) The effects of bismuth and tin on the mechanochemical processing of aluminum-based composites for hydrogen generation purposes. *Int J Hydrogen Energ* 44: 21896–21912.
28. Irankhah A, Fattahi SMS, Salem M (2018) Hydrogen generation using activated aluminum/water reaction. *Int J Hydrogen Energ* 43: 15739–15748.
29. Suryanarayana C (2001) Mechanical alloying and milling. *Prog Mater Sci* 46: 1–184.

30. Saceleanu F, Vuong TV, Master ER, et al. (2019) Tunable kinetics of nanoaluminum and microaluminum powders reacting with water to produce hydrogen. *Int J Energ Res* 43: 7384–7396.
31. Salazar M, Pérez R, Rosas G (2005) Environmental embrittlement characteristics of the AlFe and AlCuFe intermetallic systems. *J New Mater Electrochem Syst* 8: 97–100.
32. Krasnowski M, Gierlotka S, Ciołek S, et al. (2019) Nanocrystalline NiAl intermetallic alloy with high hardness produced by mechanical alloying and hot-pressing consolidation. *Adv Powder Technol* 30: 1312–1318.
33. Naghiha H, Movahedi B, Asadabad MA, et al. (2017) Amorphization and nanocrystalline Nb3Al intermetallic formation during mechanical alloying and subsequent annealing. *Adv Powder Technol* 28: 340–345.
34. Antipina SA, Zmanovskii SV, Gromov AA, et al. (2017) Air and water oxidation of aluminum flake particles. *Powder Technol* 307: 184–189.
35. Wang HW, Chung HW, Teng HT, et al. (2011) Generation of hydrogen from aluminum and water-effect of metal oxide nanocrystals and water quality. *Int J Hydrogen Energ* 36: 15136–15144.
36. Gai WZ, Deng ZY (2014) Effect of trace species in water on the reaction of Al with water. *Journal Power Sources* 245: 721–729.
37. Ma GL, Dai HB, Zhuang DW, et al. (2012) Controlled hydrogen generation by reaction of aluminum/sodium hydroxide/sodium stannate solid mixture with water. *Int J Hydrogen Energ* 37: 5811–5816.
38. Xu S, Zhao X, Liu J (2018) Liquid metal activated aluminum-water reaction for direct hydrogen generation at room temperature. *Renew Sust Energ Rev* 92: 17–37.
39. Nie H, Schoenitz M, Dreizin EL (2012) Calorimetric investigation of the aluminum–water reaction. *Int J Hydrogen Energ* 37: 11035–11045.
40. Belete TT, Van De Sanden MCM, Gleeson MA (2019) Effects of transition metal dopants on the calcination of $CaCO_3$ under Ar, H_2O and H_2. *J CO_2 Util* 31: 152–166.
41. Liu H, Yang F, Yang B, et al. (2018) Rapid hydrogen generation through aluminum-water reaction in alkali solution. *Catal Today* 318: 52–58.
42. Soler L, Candela AM, Macanás J, et al. (2009) Hydrogen generation by aluminum corrosion in seawater promoted by suspensions of aluminum hydroxide. *Int J Hydrogen Energ* 34: 8511–8518.
43. Xiao F, Guo Y, Li J, et al. (2018) Hydrogen generation from hydrolysis of activated aluminum composites in tap water. *Energy* 157: 608–614.
44. Wang CC, Chou YC, Yen CY (2012) Hydrogen Generation from aluminum and aluminum alloys powder. *Procedia Eng* 36: 105–113.

AIMS Press